A Physically Based Parameter Extraction Scheme for SCR Models

L. Göhler, T. Langer*, J. Sigg*

Universität der Bundeswehr München, Werner-Heisenberg-Weg 39, D-85577 Neubiberg, Germany
Tel.: +49-89-6004-3665, Fax: +49-89-6004-2223, email: goehler@e4s21.et.unibw-muenchen.de
*Siemens AG, Corporate Technology, Munich, Germany

Abstract–This paper presents a physically based parameter extraction scheme for SCR models. The methods are discussed and demonstrated with an example. The comparison between simulated and measured device behaviour shows agreement within 15% tolerance.

I. Introduction

In recent years research has been concentrated on the development of power device models, but very often parameter determination was not considered sufficiently. These values were assumed to be given, although even the manufacturer can not provide all required information. Therefore the focus of this paper is directed towards this deficit.

Pure curve-fitting (automated or by trial and error) of a given model to measured transients and DC-characteristics may lead to satisfying results, but there is still an uncertainity, whether the initial values of that optimization are precise enough to obtain a parameter set, which allows the model to reproduce the whole range of operation.

For comparatively simple models with only a few not very complex equations one can use derivations of these model equations for extraction [1]. Normally there is no further refinement of the parameter set necessary. In contrast, most more accurate models consist of a large number of equations (explicit and implicit) or are completely numerical. In this case it is of utmost importance to derive appropriate measurement methods for parameter determination.

All extraction methods described in the following are non-destructive and require electrical measurements only.

II. Parameter Extraction Scheme

A. Parameter Set

The parameter set, consisting of 15 parameters, corresponds to the model of a cathode-shorted SCR in [2] (see Fig. 1 and Table I).

TABLE I
Parameter Set

Parameter	Physical Meaning
A	Active area
N_{b1}	Doping of the n-base
N_{b2}	Peak doping of the p-base
N_{e1}	Peak doping of the p-emitter
N_{e2}	Peak doping of the n-emitter
w_{b1}	Width of the n-base
w_{b2}	Width of the p-base
w_{e1}	Width of the p-emitter
w_{e2}	Width of the n-emitter
τ_{b1}	Minority carrier lifetime (n-base)
τ_{b2}	Minority carrier lifetime (p-base)
I_{se1}	Saturation current (elec. inj., p-emitter)
I_{se2}	Saturation current (hole inj., n-emitter)
R_s	Short resistance
V_{brga}	Breakdown voltage (n^-p-junction)

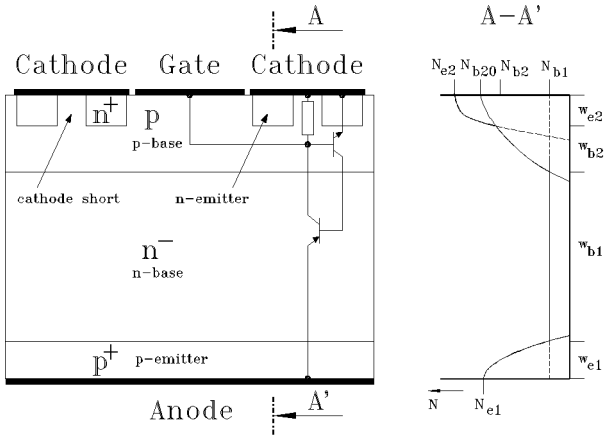

Fig. 1. Structure of a cathode-shorted SCR with equivalent circut and doping profile.

Additional values, such as thermal resistances and capacities, are taken from the data book.

B. Extraction of Doping Parameters

By measuring the capacitance C_j of the reverse biased middle junction the uniform n-base doping and the doping profile parameters of the p-base can be extracted (Fig. 2).

Since the positive anode-gate bias voltage V_r forces the p-emitter-n-base junction in forward mode its capacity has a considerably larger value than C_j. Consequently, the resulting capacity equals C_j in good approximation.

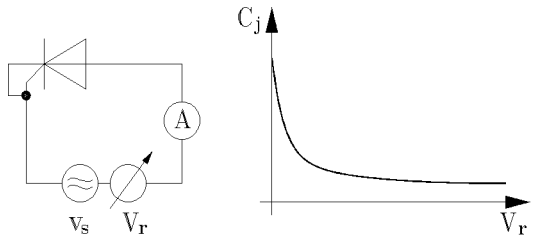

Fig. 2. Junction capacitance measurement.

Measured C_j (V_r) data are transferred to a device simulator with a built-in optimizer, such as MEDICI, to get the doping parameters N_{b1}, N_{b20} (p-doping at peak emitter doping), A and the sum of p-base and n-emitter width $w_{b2} + w_{e2}$. As the SCR model presupposes a Gaussian p-base doping profile this profile type should be selected in the device simulator, too. The less dimensions optimization has the easier a solution is found. Assuming that N_{b1} dominates C_j at the maximum V_r gives the opportunity to save one dimension:

$$A \approx C_{j\,min} \sqrt{\frac{2V_{r\,max}}{q\varepsilon_0\varepsilon_r N_{b1}}}. \tag{1}$$

Due to the shorts $w_{b2} + w_{e2}$ can not be splitted into w_{e2} and w_{b2}, but usually w_{e2} is smaller than w_{b2} and not wider than $20\mu m$. N_{e2} may follow from estimations.

Obviously, the same procedure works for the not shorted p-emitter-n-base junction to get N_{e1} and w_{e1}.

The method described becomes more complicated with increasing device dimensions. This means no disadvantage in practice, because in case of high power devices the doping profile is very well known.

As an alternative to device simualtions the approximation

$$\exp\left(-\frac{x^2}{\lambda^2}\right) \approx \frac{a_1}{1 + \exp\left(\frac{a_2}{\lambda}x + a_3\right)} \tag{2}$$

allows to calculate the capacity of a diffused layer junction (a_1, a_2, a_3=const.). Based on that, a suitable optimizer, such as CYNOSURE, performes the least-square fit.

C. Determination of the Breakdown Voltage

The middle junction is reverse biased again (Fig. 3). V_{brga} equals that voltage the anode current starts to increase rapidly for.

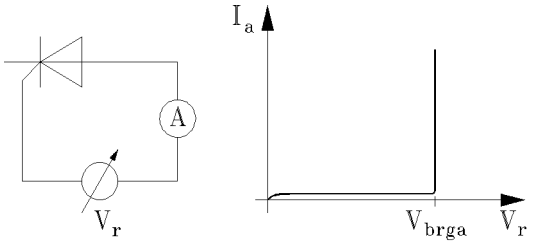

Fig. 3. Breakdown voltage measurement.

D. Determination of the n *-Base Lifetime*

In forward conduction mode electrons and holes are stored in the n- and p-base (Fig. 4, $Q_{b1} \gg Q_{b2}$). During turn-off extraction and recombination reduce excess carrier concentration until the device blocks. In case of no injection into the emitters charge control equation describes the charge decrease in the form:

$$i_a = \frac{Q_{b1}}{\tau^*_{an}} + \frac{dQ_{b1}}{dt}. \tag{3}$$

The variable i_a denotes the anode current and τ^*_{an} stands for the current-dependent high-level injection lifetime. Applying active or passive commutation (Fig. 5) the current waveform can be approximated by linear and sinusoidal functions (Fig. 6), so that (3) becomes integrable.

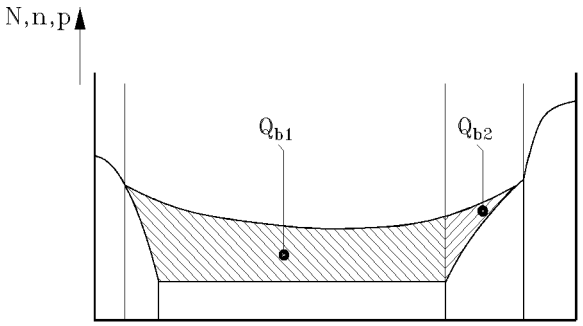

Fig. 4. Charge in the n-base and the p-base under static conditions ($Q_{b1} \gg Q_{b2}$).

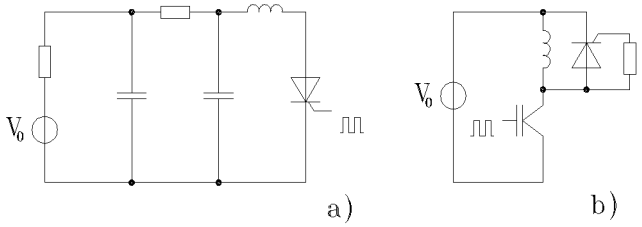

Fig. 5. Measuring circuits for passive (a) and active (b) commutation.

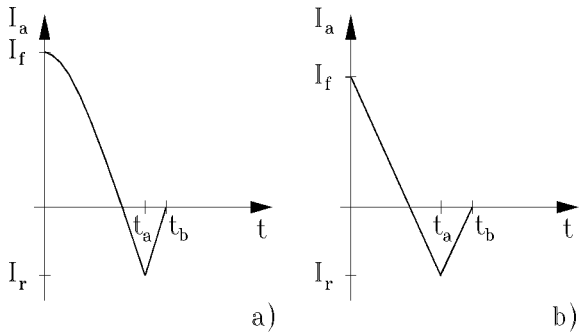

Fig. 6. Current waveforms for passive (a) and active (b) commutation.

With $Q_{b1}(t=0) = I_f \tau_{an}^*$ and $Q_{b1}(t=t_b) = 0$ the value of τ_{an}^* follows from active

$$0 = \left(\frac{I_f}{I_r} - 1\right)\left(1 - \exp\left(-\frac{t_a}{\tau_{an}^*}\right)\right) \times \left(\frac{t_b}{t_a} - 1\right) + \exp\left(\frac{t_b - t_a}{\tau_{an}^*}\right) - 1 \quad (4)$$

or passive commutation:

$$0 = -1 - \left(\frac{\tau_{an}^*}{t_b - t_a} + 1\right)\left(\exp\left(-\frac{t_b - t_a}{\tau_{an}^*}\right) - 1\right) + \frac{I_f}{I_r}\frac{\exp\left(-\frac{t_b}{\tau_{an}^*}\right)}{1 + \omega^2 \tau_{an}^{*2}}\left(\omega^2 \tau_{an}^{*2} + \exp\left(\frac{t_a}{\tau_{an}^*}\right) \times (\cos(\omega t_a) + \omega \tau_{an}^* \sin(\omega t_a))\right). \quad (5)$$

Due to emitter backinjection τ_{an}^* depends on the anode current. Hence, τ_{b1} equals the limit of τ_{an}^* for $I_f \to 0$:

$$\tau_{b1} \approx 0.5 \lim_{I_f \to 0} \tau_{an}^*. \quad (6)$$

The factor 0.5 derives from Shockley-Read-Hall recombination formula for equal minority carrier liftime in n- and p-silicon. Commutation speed has minor influence on active commutation only. For passive commutation the assumption of static conditions at $I(t) = I_f$ is not tenable at high frequencies.

E. Determination of the n *-Base Width*

The small signal behaviour of the gate-anode pnp-transistor offers a comfortable way to obtain w_{b1}. Fig. 7 presents the equivalent circuit under these conditions. Both junctions are modelled by a capacity and a resistor connected by the n-base resistance R_{b1}.

For a neglectable small value of the parasitic capacity C_σ one gets:

$$R_{b1} = \frac{1}{q N_{b1} \mu_n} \frac{w_{b1}}{A} = \lim_{\omega \to \infty} R_{measure}(\omega), \quad (7)$$

otherwise R_{b1} results from a comparison of the resistance measured at different frequencies with the frequency behaviour according to Fig. 7.

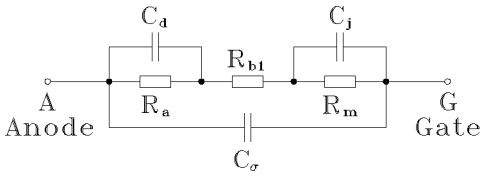

Fig. 7. Small signal model of the gate-anode structure (C_d diffusion capacity p^+n^--junction, R_a differential resistance p^+n^--junction, R_{b1} n-base resistance, C_j junction capacity n^-p-junction, R_m differential resistance n^-p-junction, C_σ parasitic capacity).

As a high frequency LRC meter provides only very low currents this procedure is limited to smaller devices.

Another method considers rapid active commutation ($t_a < \frac{\tau_{an}^*}{3}$, Fig. 6b) at low currents. In a first step (4) provides a value for the current-dependent lifetime τ_{an}^*. One can then assume the charge at reverse peak current to be

$$Q(t = t_a) = q A w_{b1} p_c, \quad (8)$$

where p_c denotes the DC-excess carrier density in the n-base at the middle junction. Using (4) again, (9) gives an approximate value for w_{b1} ($L_{an} = \sqrt{2 D_{an} \tau_{b1}}$; D_{an} ambipolar diffusion constant in the n-base):

$$w_{b1} \approx 4 L_{an}\left(\frac{I_r}{I_f} + \frac{\tau_{an}^*}{t_a}\left(\exp\left(-\frac{t_a}{\tau_{an}^*}\right) - 1\right) \times \left(\frac{I_r}{I_f} - 1\right)\right). \quad (9)$$

In some cases w_{b1} corresponds to the measured breakdown voltage V_{brga}. If V_{brga} is smaller than the value expected from n-base doping, the current increases due to punch trough:

$$w_{b1} = \sqrt{\frac{2 \varepsilon_0 \varepsilon_r V_{brga}}{q N_{b1}}}. \quad (10)$$

F. Determination of the p *-Base Lifetime*

Normally the high-level injection lifetime in the n-base ($2 \cdot \tau_{b1}$) equals that in the p-base near the middle junction, but doping dependence of lifetime should not be neglected. Using the results by Roulston [4] and Scharfetter, $\tau_{b2}(x)$ becomes (Fig. 8):

$$\tau_{b2}(x) = \frac{\tau_{b20}}{1 + \frac{N(x)}{N_{ref}}} \quad (11)$$

with $\tau_{b20} \approx \tau_{b1}$ and $N_{ref} \approx 3{\cdot}10^{15}\mathrm{cm}^{-3}$. The identity of τ_{b1} and the maximum minority carrier lifetime τ_{b20} explains again from the assumption of equal lifetime in n- and p-type silicon.

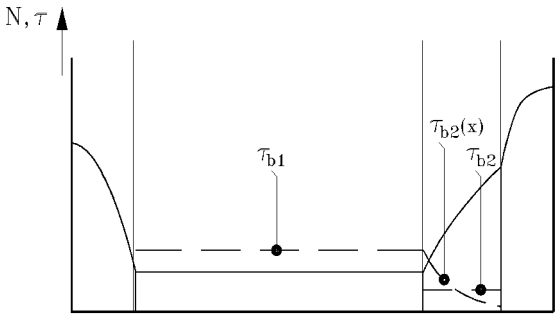

Fig. 8. Minority carrier lifetime in the n-base and the p-base.

A common approach for the effective p-base lifetime evaluates the integral of $1/\tau_{b2}(x)$ over w_{b2}:

$$\frac{1}{\tau_{b2}} = \frac{1}{w_{b2}} \int_{w_{e2}}^{w_{e2}+w_{b2}} \frac{dx}{\tau_{b2}(x)}, \tag{12}$$

expressing, that the recombination term in the ambipolar diffusion equation does not change when using the effective lifetime instead of the doping dependent one. Inserting (2) into (12) leads to:

$$\begin{aligned} \frac{1}{\tau_{b2}} &= \frac{1+\frac{N_{b1}}{N_{ref}}}{\tau_{b1}} + \frac{a_1 \lambda N_{b20}}{a_2 w_{b2} \tau_{b1} N_{ref}} \ln(f_1), \qquad (13) \\ f_1 &= \frac{1+\exp\left(-\frac{a_2}{\lambda} w_{e2} - a_3\right)}{1+\exp\left(-\frac{a_2}{\lambda}(w_{e2}+w_{b2}) - a_3\right)}. \end{aligned}$$

G. Determination of Sat. Currents and Short Resistance

With known emitter doping profiles device simulations of the interesting p-n-junctions are an elegant way to obtain the saturation currents.

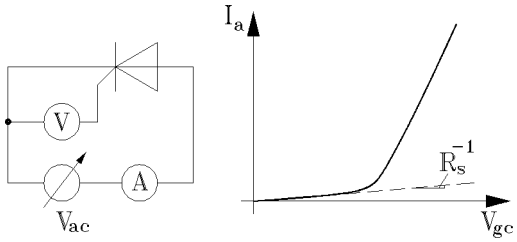

Fig. 9. Measuring the anode current as a function of gate-cathode voltage.

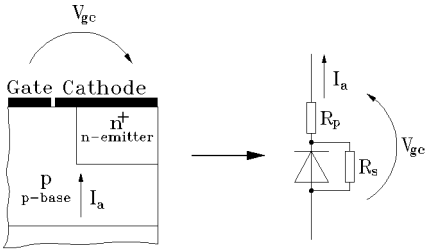

Fig. 10. Thyristor structure and equivalent circuit for $I_a = f(V_{gc})$ measurement.

Alternatively, the anode current of the ignited thyristor is plotted versus the gate-cathode voltage (Fig. 9, 10). The saturation currents of backinjection are obtained by fitting this curve to the model equations in static case for both the p^+n^- and the n^-p-junction. This method facilitates to ignore the base resistance and forces the current to flow along the main current path. Measuring the characteristic dynamically limits self-heating of the device. Fig. 10 shows the SCR's cathode region and the corresponding circuit.

Equation (14) results for the short resistance at low anode currents, because $R_s \gg R_p$.

$$R_s \approx \frac{V_{gc}}{I_a} \tag{14}$$

The v-i-characteristic of the n-emitter-p-base-junction has the following form (D_n diffusion constant for electrons, L_{ap} ambipolar diffusion length in the p-base):

$$\begin{aligned} I_a &= \left(\frac{2qAD_n n_i^2}{N_{b2} L_{ap} \tanh\left(\frac{w_{b2}}{L_{ap}}\right)} + I_{se2}\right) \times \\ &\quad \left(\exp\left(\frac{V_{gc}^*}{mV_T}\right) - 1\right) + \left(1 + \frac{\mu_n}{\mu_p}\right) I_{se2} \frac{n_i^2}{N_{b2}^2} \times \\ &\quad \left(\exp\left(\frac{2V_{gc}^*}{mV_T}\right) - 1\right), \qquad (15) \end{aligned}$$

which can be transformed to take into account the parasitic resistance R_p (V_T: thermal voltage):

$$\begin{aligned} V_{gc} &= mV_T \ln(f_0) + I_a R_p, \qquad (16) \\ f_0 &= \frac{f_1}{2f_2}\left(\sqrt{1 + \frac{4f_2^2}{f_1^2}\left(\frac{f_1}{f_2} + \frac{I_a}{f_2} + 1\right)} - 1\right), \\ f_1 &= \frac{2qAD_n n_i^2}{N_{b2} L_{b2} \tanh\left(\frac{w_{b2}}{L_{b2}}\right)} + I_{se2}, \\ f_2 &= \left(1 + \frac{\mu_n}{\mu_p}\right) I_{se2} \frac{n_i^2}{N_{b2}^2}. \end{aligned}$$

This leads to I_{se2}, R_p and m (in case of a low short resistance it should be subtracted before). The function

of m is to incorporate the remaining self-heating. With the eliminated voltage drop due to R_p a least-square fit of that curve to the anode current as a function of V_{am} (effective voltage across p-emitter-n-base junction) yields I_{se1}:

$$I_a = \frac{2qAD_p n_i^2}{N_{b1} L_{an} \tanh\left(\frac{w_{b1}}{L_{an}}\right)} \left(\exp\left(\frac{V_{am}}{mV_T}\right) - 1\right) + \left(1 + \frac{\mu_p}{\mu_n}\right) I_{se1} \frac{n_i^2}{N_{b1}^2} \times \left(\exp\left(\frac{2V_{am}}{mV_T}\right) - 1\right). \quad (17)$$

The difference between V_{gc}^* and V_{am} may be seen as constant:

$$V_{am} \approx V_{gc}^* - V_d \quad (18)$$

III. Results

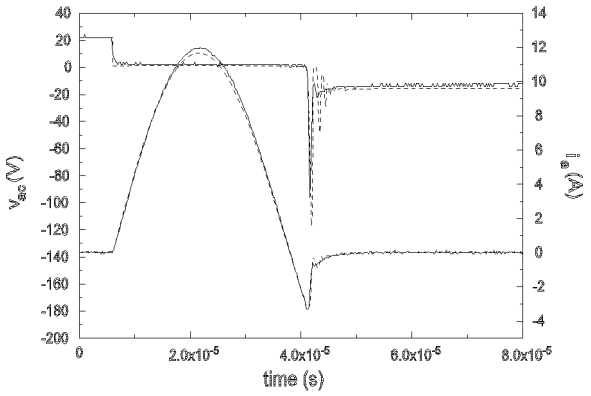

Fig. 11. Comparison between measurement (—) and simulation (- -) of passive commutation with manufacturer/fitted data.

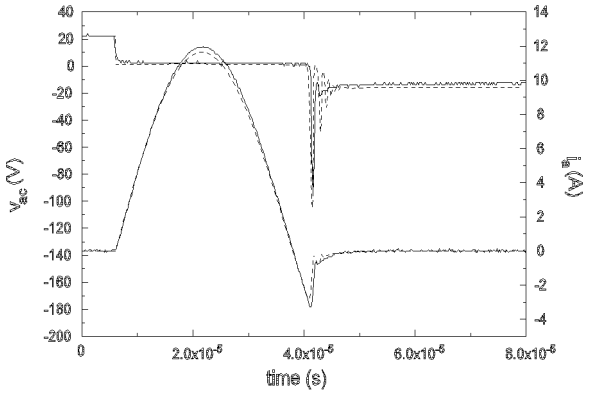

Fig. 12. Comparison between measurement (—) and simulation (- -) of passive commutation with extracted parameters.

TABLE II
Comparison between Manufacturer/Fitted Data and Extracted Parameters

Parameter	Manufacturer/Fit	Extracted
$A(cm^2)$	0.03	0.037
$N_{b1}(cm^{-3})$	$2 \cdot 10^{14}$	$1.7 \cdot 10^{14}$
$N_{b2}(cm^{-3})$	$4 \cdot 10^{16}$	$2.7 \cdot 10^{16}$
$N_{e1}(cm^{-3})$	$1 \cdot 10^{17}$	$9 \cdot 10^{16}$
$N_{e2}(cm^{-3})$	$5 \cdot 10^{19}$	$1 \cdot 10^{19}$
$w_{b1}(\mu m)$	156	173
$w_{b2}(\mu m)$	18	28
$w_{e1}(\mu m)$	38	49
$w_{e2}(\mu m)$	18	20
$\tau_{b1}(\mu s)$	4	3.5
$\tau_{b2}(\mu s)$	1	1
$I_{se1}(A)$	$0.6 \cdot 10^{-15}$	$1.8 \cdot 10^{-15}$
$I_{se2}(A)$	$9 \cdot 10^{-14}$	$9 \cdot 10^{-14}$
$R_s(\Omega)$	10	6
$V_{brga}(V)$	1000	1060

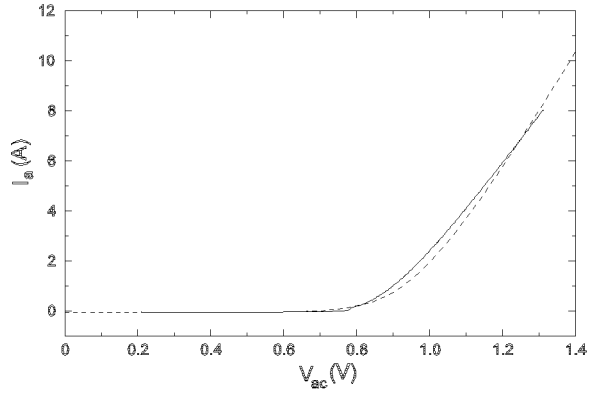

Fig. 13. Comparison between measurement (—) and simulation (- -) of DC-characteristic with manufacturer/fitted data.

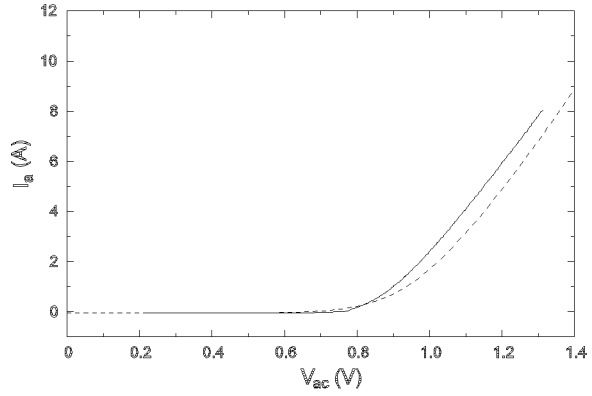

Fig. 14. Comparison between measurement (—) and simulation (- -) of DC-characteristic with extracted parameters.

All extraction routines were performed for a small thyristor ($I_{TAV} = 7.5A$) to prove the concept. In Table II a comparison is displayed between data given by the manufacturer or obtained from fitting the model to best agreement with measurement and extracted parameters.

In transient simulation (Fig. 11, 12) a reverse peak current deviation of approximately 15% occurs. The DC-current difference (Fig. 13, 14) at $I = I_{TAV}$ amounts 14%. These deviations are mainly determined by the different values of τ_{b1} and I_{se1}, which lead to an increased device resistance and a reduction of the stored charge in the model compared to the device. It is clearly to be seen, that the extracted parameters meet manufacturer data.

IV. Conclusion

A physically based parameter extraction scheme for SCR models is presented. The comparison with manufacturer data proves a good agreement within 15% tolerance. Some of the procedures, such as junction capacity measurement, minority carrier lifetime determination and the extraction of n-base width can be applied to other power devices, too. All methods are destruction-free.

References

[1] H. Güldner, K. Lehnert, B. Arlt, L. Göhler, Adaptation of a Power Diode Model to PSPICE, Proc. of PCIM '95.

[2] M. Bayer, R. Kraus, K. Hoffmann, A new analytical SCR-Model for Circuit Applications, Proc. of SPEC '94.

[3] S. K. Ghandi, Semiconductor Power Devices, John Wiley & Sons, Inc., 1977.

[4] D. J. Roulston, N. D. Arora, S. G. Chamberlain, Modeling and Measurement of Minority-Carrier Lifetime versus Doping in Diffused Layers of $n^+ - p$ Silicon Diodes, IEEE Trans. on Electron Devices, vol. 29, No. 2, February 1982.